

Complex Raman Tensor in Helicity-Changing Raman Spectra of Black Phosphorus under Circularly Polarized Light

Shiyi Han, Yan Zhao, Nguyen Tuan Hung, Bo Xu, Riichiro Saito,* Jin Zhang, and Lianming Tong*

Cite This: *J. Phys. Chem. Lett.* 2022, 13, 1241–1248

Read Online

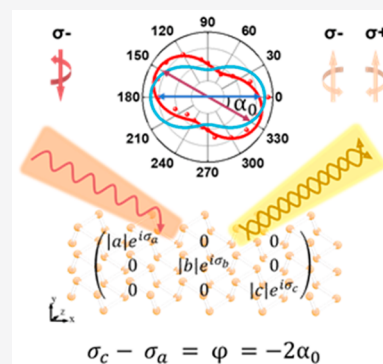
ACCESS |

Metrics & More

Article Recommendations

Supporting Information

ABSTRACT: In anisotropic two-dimensional materials, complex values of Raman tensors are necessary to explain the abnormal linearly polarized Raman spectra. In this work, we measured the helicity-changing Raman spectra of few-layer black phosphorus (BP) excited by circularly polarized light. We observed that the polarized Raman intensities of the A_g modes show a deflection angle that depends on the sample orientation, thickness, and laser excitation energy. To understand the deflection, we calculated the resonant Raman spectra by first-principles calculations, which give complex Raman tensors as a function of laser excitation energy. In particular, the phase difference between the elements of the complex Raman tensor is relevant to the deflection angle. The calculated results of monolayer BP reproduce the experimental helicity-resolved Raman spectra of few-layer BP satisfactorily.



Black phosphorus (BP) is a layered semiconductor material.¹ The puckered structure relaxes restriction for the bond angle, which makes BP the most stable allotrope among the phosphorus materials.^{1–6} The bulk structure of BP has an orthorhombic symmetry belonging to point (space) group D_{2h} ($Cmca$). Thus, the crystal structure has in-plane anisotropy that is relevant to the optical properties of BP.^{1,3} Because monolayer and multilayer BP are direct band gap semiconductors,^{5,7,8} we can discuss the optical properties of BP as a function of the thickness of BP. Because the energy gap decreases with an increase in the number of layers and we expect many energy subbands near the Fermi energy, we can control the optical properties of BP for photonic and optoelectronic applications.^{6,9,10}

Resonant Raman spectroscopy is a nondestructive characterization tool for analyzing the electronic and phonon structure of low-dimensional materials. In particular, when we use circularly polarized light (CPL), we can analyze the symmetry of phonon modes by helicity-dependent Raman spectroscopy,¹¹ in which the helicity of the scattered CPL either is conserved or changes from that of the incident CPL depending on the phonon mode.¹² For example, the G-band of graphene¹³ and the in-plane E mode of transition metal dichalcogenides (TMD) such as MoS_2 ^{14,15} are helicity-changing Raman modes, while the out-of-plane A mode of TMD is a helicity-conserved Raman mode. We can generally explain the helicity-changing or helicity-conserved Raman spectra in terms of the Raman tensor.^{13,16,17}

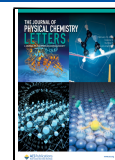
In this paper, we report the helicity-resolved Raman spectra of BP by using CPL in which we report the unique helicity-resolved behavior for the A_g mode. BP has two A_g Raman

active modes and one B_{2g} Raman active mode.^{18–21} If we adopted the real values of Raman tensors for the A_g and B_{2g} modes of BP, the A_g mode would be a helicity-conserved Raman mode if the value of the diagonal elements are the same, while the B_{2g} mode would be a helicity-changing Raman mode if the elements are non-zero. However, when we measured the polarized Raman intensities of few-layer BP excited by CPL, the angle of maximum peak intensity in the polar plot shows a deflection angle for the A_g modes. The deflection corresponds to the fact that the A_g mode of BP is not completely helicity-conserved, and the degree of deflection depends on the phonon mode, sample thickness, and laser excitation energy. Ribeiro et al.²² discussed Raman spectra of BP using linear polarized light by introducing the complex Raman tensor, in which they investigated the complex values of electron–phonon matrix elements and the energy denominator. Resende et al.²³ explained the origin of the complex Raman tensors for ReSe_2 in terms of the anisotropy of the electron–phonon coupling, also by using linearly polarized Raman spectroscopy. In this paper, by using a homemade program of resonant Raman spectra, we calculated the helicity-resolved resonant Raman spectra of monolayer BP by first principles¹³ by which we obtained the complex Raman tensor. The calculated results of the phase difference between Raman

Received: November 23, 2021

Accepted: January 25, 2022

Published: January 28, 2022



tensor elements of monolayer BP satisfactorily reproduce the observed deflection of the A_g mode of few-layer BP as a function of laser excitation energy.

In Figure 1a, we show the experimental setup of helicity-resolved Raman spectroscopy (HRRS). The atomic structure

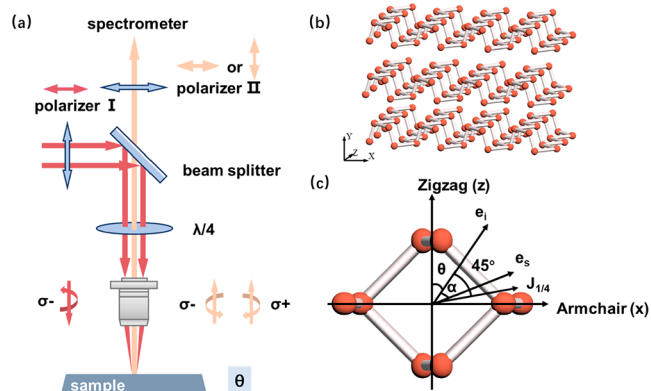


Figure 1. Experimental setup and coordinate system for a black phosphorus (BP) sample. (a) Experimental setup for helicity-resolved Raman scattering spectroscopy (HRRS). (b) Atomic structure of BP. (c) Coordinate system for the HRRS measurements.

of layered BP is shown in Figure 1b, and Figure 1c shows the coordinate system for the HRRS measurements. θ denotes the direction of the crystalline orientation of BP with respect to the polarization direction of light, where a θ of 0° or 90° corresponds to the zigzag (z) or armchair (x) edge direction, respectively. The quarter-wave plate, whose optical axis direction is set to be 45° from the polarization direction of the incident light, is placed in the optical path for generating either left-handed circularly polarized light (σ^+ , LCP) or right-handed circularly polarized light (σ^- , RCP). The back-

scattered Raman scattering light goes through the quarter-wave plate again and then another linear polarizer II whose direction between the incident light is denoted by the angle α . If we observe the Raman intensity at $\alpha = 0^\circ$ and zero intensity at $\alpha = 90^\circ$, the scattered light corresponds to helicity-conserving Raman spectra, and Raman intensity at $\alpha = 90^\circ$ and zero intensity at $\alpha = 0^\circ$ for helicity-changing Raman spectra. If we observe the Raman intensity for a general α between 0° and 90° , the scattered light is not pure LCP or RCP.

Few-layer BP samples with several thicknesses on a 300 nm SiO_2/Si substrate were prepared by using mechanical exfoliation. Figure 2a shows the atomic force microscopy (AFM) and optical microscopy (OM) images of the BP sample. The thickness of BP measured by AFM is 7 nm, which corresponds to 13 layers. In panels b and c of Figure 2, we plot the observed Raman spectra of the BP excited by 2.33 and 1.96 eV lasers, respectively, in which we observe three Raman active modes, that is, A_g^1 (363 cm^{-1}), B_{2g} (440 cm^{-1}), and A_g^2 (467 cm^{-1}). The red (blue) spectra correspond to helicity-changing (helicity-conserving) Raman spectra. As shown in panels b and c of Figure 2, the B_{2g} mode shows helicity-changing Raman spectra while the A_g modes show intensities for both $\sigma^+\sigma^+$ and $\sigma^+\sigma^-$ configurations, and the relative intensity is not the same for the two A_g modes and for the laser excitation energy.

To understand the unique helicity-resolved behavior of the A_g modes, we have calculated the electronic and phonon energy dispersions of monolayer BP by first-principles calculations, as shown in Figure S1, which assign the Raman active modes of A_g and B_{2g} modes. The A_g modes oscillate in all directions, while the B_{2g} mode oscillates only in the x - z plane (see Figure S1d). It is important to note that the x , y , and z axes of the BP are set to the conventional notation in which the in-plane direction is x , z (not x , y) and the out-of-plane direction is y (not z). Thus, the B_{2g} mode is the in-plane mode.

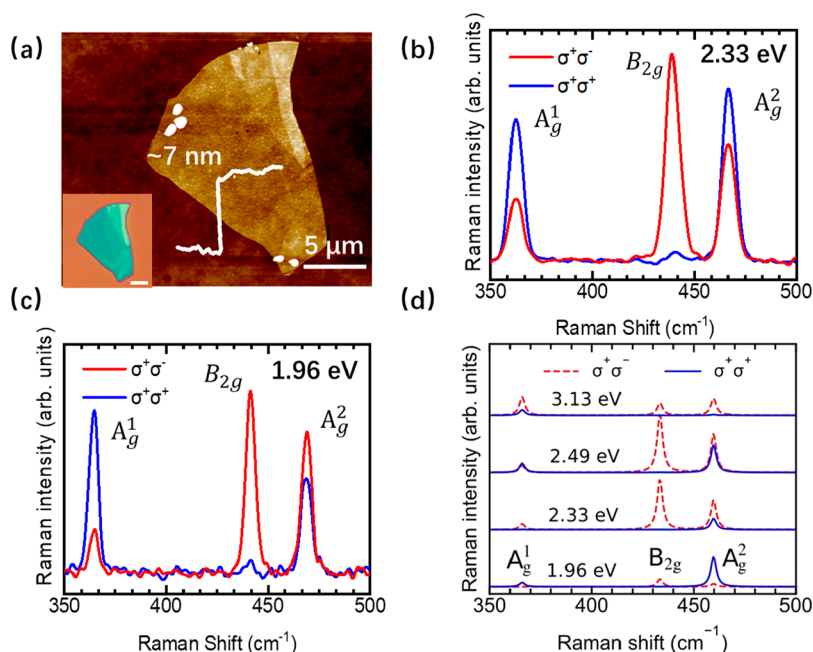


Figure 2. Optical microscopy (OM) and atomic force microscopy (AFM) characterization of a BP flake and experimental and calculated HRRS results. (a) AFM image of few-layer BP on a 300 nm SiO_2/Si substrate. The inset shows the OM image (the scale bar is $5\ \mu\text{m}$). HRRS results for A_g and B_{2g} modes of BP excited by (b) $E_L = 2.33\text{ eV}$ (532 nm) and (c) $E_L = 1.96\text{ eV}$ (633 nm) lasers. (d) Calculated helicity-dependent Raman spectra of the monolayer BP for several laser energies (1.96, 2.33, 2.49, and 3.13 eV).

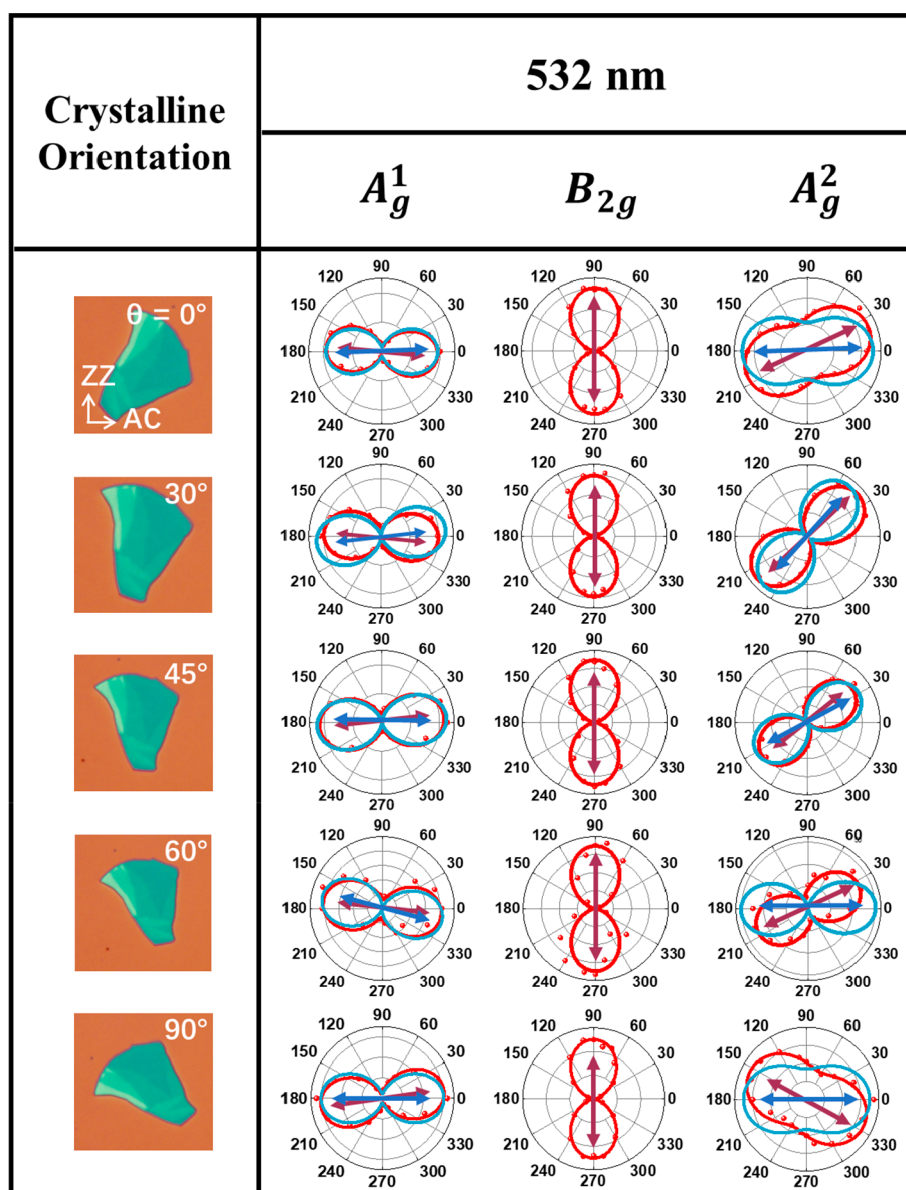


Figure 3. Circularly polarized Raman scattering of BP as a function of α with different crystalline orientations excited by an $E_L = 2.33$ eV (532 nm) laser. The red dots are the experimental data; the red curves are fits to eqs 12 and 13, and the blue curves are fits to eq 12 with $\varphi = 0^\circ$. The red and blue arrows show the direction of the maximum intensity for the red and blue curves, respectively.

In Figure 2d, we plot the calculated, helicity-dependent Raman spectra of monolayer BP for the several laser energies (1.96, 2.33, 2.49, and 3.13 eV). For the B_{2g} mode, we can see that the calculated Raman spectra show only helicity-changing ($\sigma+\sigma-$) Raman spectra (red dashed lines) for the all-excitation energies. For the A_g modes, the helicity-changing Raman spectra ($\sigma+\sigma-$) are dominant for relatively higher E_L values. For a lower E_L of 1.96 eV (or 2.49 eV), the helicity-conserved Raman spectra ($\sigma+\sigma+$, blue solid lines) are dominant versus (or comparable to) the helicity-changing Raman spectra. Although we cannot directly compare the measured Raman spectra for few-layer BP with the calculated results of monolayer BP, the relative intensity of helicity-conserved Raman spectra with respect to helicity-changing Raman spectra reproduces the experimental results satisfactorily.

Because the A_g mode shows intensities for both $\sigma+\sigma+$ and $\sigma+\sigma-$ configurations, the scattered light of the A_g mode is not pure LCP or RCP. In the following, we analyze the

polarization-resolved Raman scattering of the scattered light after it had passed polarizer II by using a complex Raman tensor.

The Raman intensity is expressed by the Raman tensor \mathbf{R} as follows

$$I \propto |\sigma_s^\dagger \cdot \mathbf{R} \cdot \sigma_i|^2 \quad (1)$$

where σ_i (σ_s^\dagger) denotes the Jones vector of incident (scattered) light. The Jones vectors of LCP and RCP are given by

$$\sigma_+ = \frac{1}{\sqrt{2}} \begin{pmatrix} 1 \\ 0 \\ i \end{pmatrix}, \text{ and } \sigma_- = \frac{1}{\sqrt{2}} \begin{pmatrix} 1 \\ 0 \\ -i \end{pmatrix} \quad (2)$$

The Raman tensors for the A_g mode and the in-plane B_{2g} (xz) mode are as follows.²²

$$\mathbf{R}_{A_g} = \begin{pmatrix} |a|e^{i\sigma_a} & 0 & 0 \\ 0 & |b|e^{i\sigma_b} & 0 \\ 0 & 0 & |c|e^{i\sigma_c} \end{pmatrix} \quad (3)$$

$$\mathbf{R}_{B_{2g}} = \begin{pmatrix} 0 & 0 & f \\ 0 & 0 & 0 \\ f & 0 & 0 \end{pmatrix} \quad (4)$$

We note that the xz and zx components of $\mathbf{R}_{B_{2g}}$, f , should be the same even though we consider the anisotropy. For the A_g modes, on the contrary, the xx and zz components of the Raman tensor elements are not equivalent ($|a| \neq |c|$) and they have different phases ($\sigma_a \neq \sigma_c$).

The phases of σ_a , σ_b , and σ_c can be described by nonresonant Raman theory²²

$$\sigma_a = \text{artg} \left(\frac{\frac{\partial \epsilon''_{xx}}{\partial q^{A_g}}}{\frac{\partial \epsilon'_{xx}}{\partial q^{A_g}}} \right), \sigma_b = \text{artg} \left(\frac{\frac{\partial \epsilon''_{yy}}{\partial q^{A_g}}}{\frac{\partial \epsilon'_{yy}}{\partial q^{A_g}}} \right), \sigma_c = \text{artg} \left(\frac{\frac{\partial \epsilon''_{zz}}{\partial q^{A_g}}}{\frac{\partial \epsilon'_{zz}}{\partial q^{A_g}}} \right) \quad (5)$$

where ϵ''_{ij} and ϵ'_{ij} are the imaginary and real parts, respectively, of the ij ($ij = xx, y, zz, xz$) component of the polarizability tensor and q denotes the atomic displacement of the phonon mode.

Before discussing the Raman intensity for the geometry of Figure 3, we first consider the Raman intensity without polarizer II. In Figure S2, we show the polar plots for $\sigma+\sigma+$ and $\sigma+\sigma-$ geometries without polarizer II as a function of sample orientation θ . In this case, the results should not depend on the sample orientation, because Raman spectra are excited by the CPL. Using eqs 1–4, we obtain the Raman intensities of the A_g mode for $\sigma+\sigma+$ and $\sigma+\sigma-$ geometries as follows

$$I_{A_g}^{\sigma+\sigma+} \propto \frac{||a| + |c| \cdot e^{i\varphi}|^2}{4} \text{ and } I_{A_g}^{\sigma+\sigma-} \propto \frac{||a| - |c| \cdot e^{i\varphi}|^2}{4} \quad (6)$$

where φ is the phase difference described as

$$\varphi = \sigma_c - \sigma_a \quad (7)$$

When we consider in-plane anisotropy ($|a| \neq |c|$), we have non-zero values for both $I_{A_g}^{\sigma+\sigma+}$ and $I_{A_g}^{\sigma+\sigma-}$. Thus, the condition under which $|a| \neq |c|$ is sufficient to produce intensities for both $\sigma+\sigma+$ and $\sigma+\sigma-$ configurations, though the intensities depend on φ . If we assumed $|a| = |c|$ and $\varphi = 0$, we would obtain only the helicity-conserved Raman spectra. With respect to the B_{2g} mode, the Raman intensities for the $\sigma+\sigma+$ and $\sigma+\sigma-$ configurations are given by

$$I_{B_{2g}}^{\sigma+\sigma+} \propto 0 \text{ and } I_{B_{2g}}^{\sigma+\sigma-} \propto |f|^2 \quad (8)$$

Thus, the B_{2g} mode is only helicity-changing, which is consistent with the observed results.

As the A_g mode is not pure LCP or RCP, we now consider the polarized Raman intensities after passing linear polarizer II as shown in Figure 3. We will show how to obtain φ from this configuration. Because both the incident light and scattered light pass through the quarter-wave plate, the Raman intensity is expressed by

$$I \propto |(\mathbf{J}_{1/4} \cdot \mathbf{e}_s)^\dagger \cdot \mathbf{R} \cdot (\mathbf{e}_i \cdot \mathbf{J}_{1/4})|^2 \quad (9)$$

where \mathbf{e}_i (\mathbf{e}_s) refers to the Jones vector of linear polarized light of the incident (scattered) light after passing linear polarizer I (II) and $\mathbf{J}_{1/4}$ refers to the Jones vector of the quarter-wave plate. Because we define θ as the angle of the incident linear polarization \mathbf{e}_i measured from the direction of the zigzag edge of BP and α as the angle of scattered polarization measured from the angle of \mathbf{e}_i (Figure 1c), \mathbf{e}_i and \mathbf{e}_s can be given by

$$\mathbf{e}_i = \begin{pmatrix} \sin \theta \\ 0 \\ \cos \theta \end{pmatrix} \text{ and } \mathbf{e}_s = \begin{pmatrix} \sin(\alpha + \theta) \\ 0 \\ \cos(\alpha + \theta) \end{pmatrix} \quad (10)$$

The Jones vector for the quarter-wave plate is given by rotating the optical axis by $\theta + \pi/4$ ²⁴

$$\begin{aligned} \mathbf{J}_{1/4} &= \mathbf{A}^* \cdot \mathbf{J}_{1/4} \cdot \mathbf{A} \\ &= \begin{bmatrix} \cos\left(\theta + \frac{\pi}{4}\right) & 0 & \sin\left(\theta + \frac{\pi}{4}\right) \\ 0 & 1 & 0 \\ -\sin\left(\theta + \frac{\pi}{4}\right) & 0 & \cos\left(\theta + \frac{\pi}{4}\right) \end{bmatrix} \cdot \begin{pmatrix} 1 & 0 & 0 \\ 0 & 0 & 0 \\ 0 & 0 & -i \end{pmatrix} \cdot \begin{bmatrix} \cos\left(\theta + \frac{\pi}{4}\right) & 0 & -\sin\left(\theta + \frac{\pi}{4}\right) \\ 0 & 1 & 0 \\ \sin\left(\theta + \frac{\pi}{4}\right) & 0 & \cos\left(\theta + \frac{\pi}{4}\right) \end{bmatrix} \\ &= \frac{1}{2} \begin{bmatrix} 1 - \sin 2\theta - i(1 + \sin 2\theta) & 0 & -\cos 2\theta - i \cos 2\theta \\ 0 & 0 & 0 \\ -\cos 2\theta - i \cos 2\theta & 0 & 1 + \sin 2\theta - i(1 - \sin 2\theta) \end{bmatrix} \end{aligned} \quad (11)$$

Using eqs 3, 4, and 9–11, we obtain the Raman intensities of the A_g and B_{2g} modes as a function of θ and α as follows.

$$\begin{aligned} I_{A_g} &\propto \frac{1}{8} \{ (|a|^2 - |c|^2) [\sin^2(\alpha + \theta) - \sin^2(\alpha - \theta)] + |a|^2 \\ &\quad + |c|^2 - 2|a||c| [\sin(\varphi) \sin(2\alpha) \cos(2\theta) - \cos(2\alpha) \\ &\quad \times \cos(\varphi)] \} \end{aligned} \quad (12)$$

$$I_{B_{2g}} \propto |f|^2 \sin^2(\alpha) \quad (13)$$

It is clear that the intensity of the B_{2g} modes has a maximum at $\alpha = 90^\circ$, which is consistent with the experiment. For the A_g modes, eq 12 gives a maximum intensity for a general α .

In Figure 3, we plot the observed polarized Raman intensity (red dots) of BP with a thickness of 7 nm as a function of α , for several values of crystal orientation θ . Figure 3 corresponds

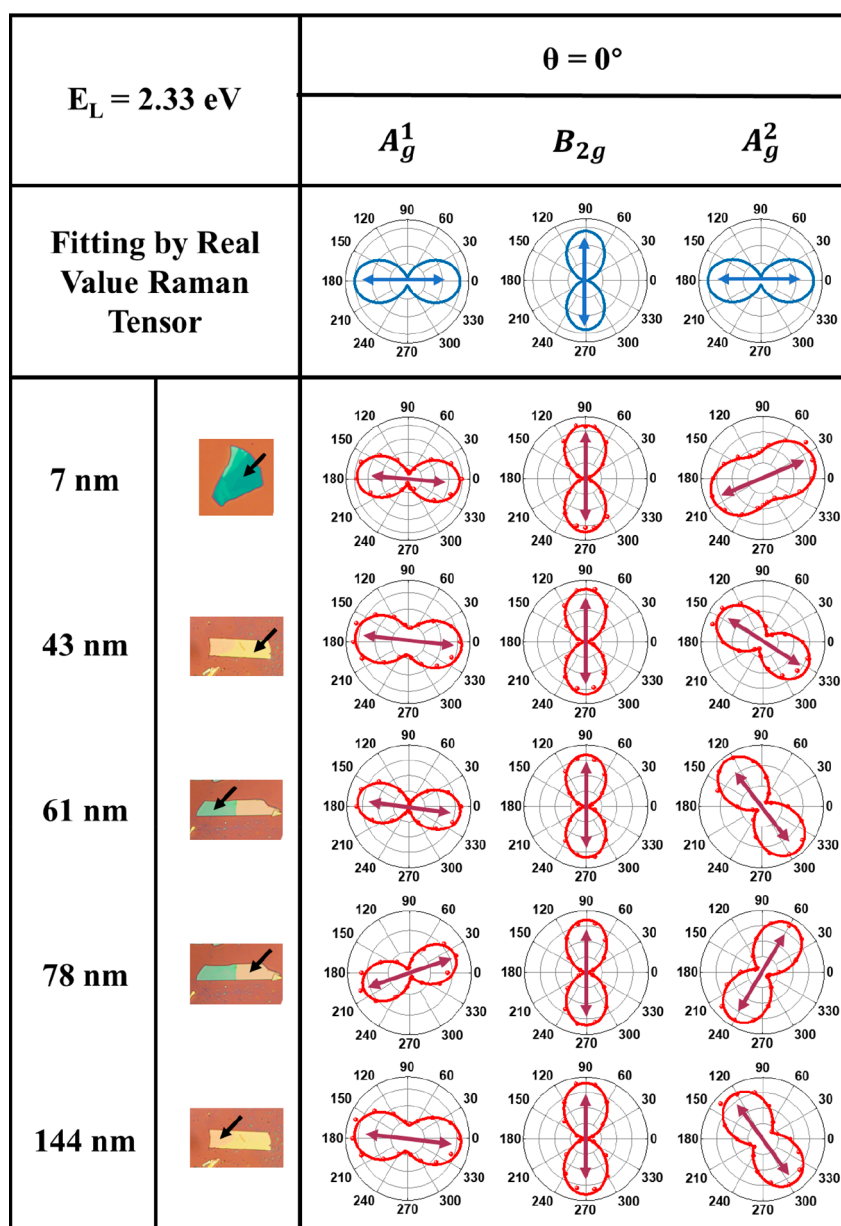


Figure 4. Polarized Raman signal of BP flakes with thicknesses of 7, 43, 61, 78, and 144 nm as a function of the angle of polarizer II. The spectra were recorded with an $E_L = 2.33 \text{ eV}$ (532 nm) laser. The sample orientation is set to be $\theta = 0^\circ$. The red curves are fits to eqs 12 and 13. The blue curves are fits to eqs 12 and 13 with $\varphi = 0^\circ$.

to 532 nm laser excitation, and the experimental data recorded with a 633 nm laser are shown in Figure S3. The red curves are fits to eqs 12 and 13 for the A_g modes and the B_{2g} mode, respectively, while the blue curves are fits to eq 12 with $\varphi = 0^\circ$. The red and blue arrows show the direction of the maximum intensity for the red and blue curves, respectively. We can see that the red curves reproduce the observed Raman intensity.

For the B_{2g} mode, because the observed polar plot intensity reaches its maximum at $\alpha = 90^\circ$, the B_{2g} mode gives helicity-changing Raman spectra, which is consistent with eq 13. However, the A_g modes appear at both 0° and 90° , which corresponds to the fact that the scattered light is now not pure LCP or RCP. The red and blue arrows in Figure 3 refer to the direction of the intensity maxima for the red and blue curves, respectively. It is clear that there is a deflection angle between the red and blue arrows. Thus, it is necessary to introduce the

complex Raman tensors to explain the deflection for the A_g modes.

In Figure 4, we show the dependence of the thickness on the polarized Raman intensity of BP for thicknesses of 7, 43, 61, 78, and 144 nm as a function of α with the sample direction fixed to $\theta = 0^\circ$. The blue lines show the results simulated by real values of the Raman tensor ($\varphi = 0$), and the red dots and curves denote the experimental data and data fitted to eq 12, respectively, where φ is involved.

In Figure S4, we show the experimental data recorded with an $E_L = 1.96 \text{ eV}$ (633 nm) laser. Compared with Figure 4, when we increase E_L , the deflection angle changes, the origin of which will be discussed further by first-principles calculations. In Figure S5, we show the polarized Raman intensity of BP for several thicknesses as a function of α at the sample orientation $\theta = 90^\circ$. Comparing Figure 4 with Figure S5, we find that the deflection angles of polarized Raman spectra have the

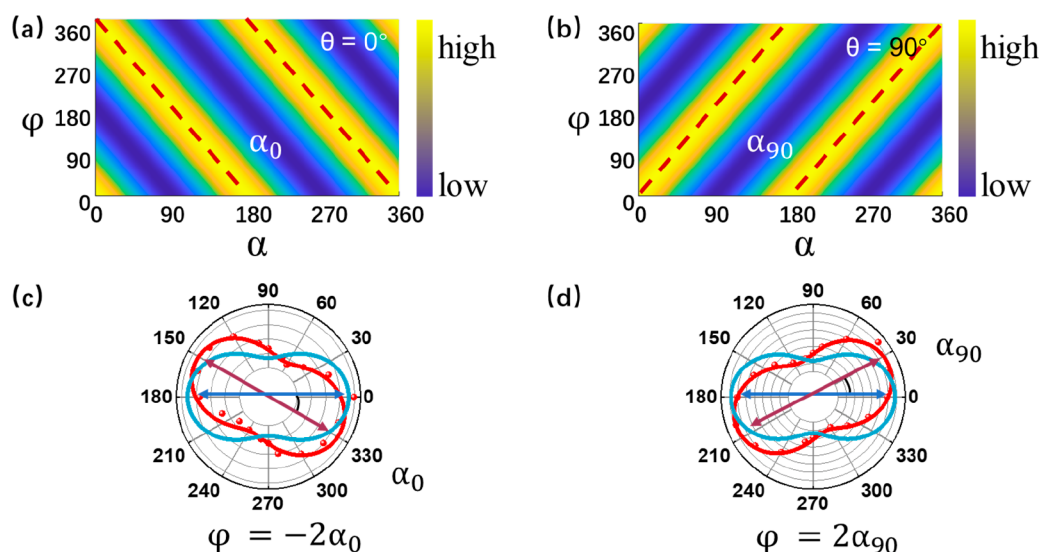


Figure 5. Illustration of the variation of the Raman intensities with rotational angle α for polarizer II and the complex phase φ when the sample orientation is (a) $\theta = 0^\circ$ or (b) $\theta = 90^\circ$. Relationship between complex phase φ and α when the sample orientation is (c) $\theta = 0^\circ$ or (d) $\theta = 90^\circ$. α_0 and α_{90} refer to the deflection angle for $\theta = 0^\circ$ and $\theta = 90^\circ$, respectively.

opposition sign for the two sample directions for $\theta = 0^\circ$ and $\theta = 90^\circ$. Interestingly, we find that the value of φ can be obtained from the deflection angle.

In particular, if we set θ equal to 0° and 90° in eq 12, we obtain

$$I_{A_g}(\theta = 0^\circ) \propto \frac{1}{8}[|a|^2 + |c|^2 + 2|a||c|\cos(2\alpha + \varphi)] \quad (14)$$

$$I_{A_g}(\theta = 90^\circ) \propto \frac{1}{8}[|a|^2 + |c|^2 + 2|a||c|\cos(2\alpha - \varphi)] \quad (15)$$

We define α as α_0 and α_{90} when the signal has a maximum Raman intensity for $\theta = 0^\circ$ and $\theta = 90^\circ$, respectively. When $\theta = 0^\circ$ and $\theta = 90^\circ$, α_0 and α_{90} have opposite signs; thus, the polar plots of Figure 4 and Figure S5 are symmetric to each other.

Panels a and b of Figure 5 show the relationship between α_0 (α_{90}) and φ ; that is, $\varphi = -2\alpha_0$ ($\varphi = 2\alpha_{90}$). In addition, α_0 (α_{90}) can be obtained by the deflection of the polar plot, which is shown in panels c and d of Figure 5. In Table S1, we show the fitted φ values for different BP thicknesses and 1.96 and 2.33 eV lasers using eq 14.

In Figure 6, we show the calculated results of the complex phase φ as a function of E_L for the A_g modes for monolayer BP. As one can see in Figure 6, the values of φ for A_g^2 are larger than those for A_g^1 , which is consistent with the fitted φ values listed in Table S1. When φ is large, we obtain a large shift in

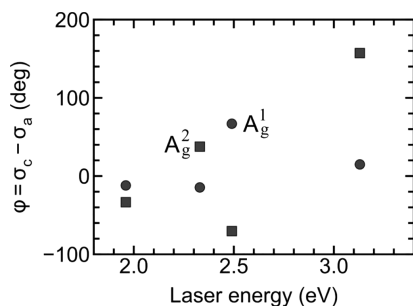


Figure 6. Calculated phase difference φ plotted as a function of laser energy for the A_g^2 and A_g^1 modes for monolayer BP.

the angle in the polar plot, which is consistent with the Raman tensor analysis. We can also see that the value of the A_g^1 mode is larger for 2.33 eV excitation than for 1.96 eV excitation, and the values of the A_g^2 mode also agree well with experimental results. Although the calculated results reproduce the E_L dependence of the relative intensity and polarized Raman spectra for the two A_g modes as a function of E_L , we should mention that the fitted φ values for some E_L values are not consistent with the calculated results. The possible reason for the discrepancy might be the fact that the calculation is for monolayer BP and the measurement is for multilayer BP. In addition, we adopted the assumption that the lifetime of the photoexcited electron does not depend on E_L . Evaluating the lifetime of the photoexcited carrier is difficult because we should consider all possible electron–phonon matrix elements even though we take the electron–phonon interaction into account. Nevertheless, the overall behavior of the relative intensity of helicity-changing or -conserving Raman spectra as a function of E_L is consistent with the calculated results.

We now discuss the origin of the complex Raman tensor in the resonant Raman spectra. The resonant Raman intensity is calculated by time-dependent perturbation theory, in which the Raman scattering amplitude F is given by¹²

$$F = \sum_{i,m,m'} \frac{\langle f|\nabla| m' \rangle \langle m'| H_{\text{el-ph}} | m \rangle \langle m|\nabla| i \rangle}{(E_L - E_{mi} - i\Gamma)(E_L - \hbar\omega_\nu - E_{m'i} - i\Gamma)} \quad (16)$$

where E_L stands for the laser energy and i , m , and m' denote the initial, intermediate, and scattered states, respectively. $E_{mi} \equiv E_m - E_i$ denotes the energy difference between states m and i . $H_{\text{el-ph}}$ denotes the electron–phonon interactions, and $\langle m|\nabla| i \rangle$ and $\langle f|\nabla| m' \rangle$ correspond to the electron–photon interaction of the optical absorption and emission, respectively. $\langle m'| H_{\text{el-ph}} | m \rangle$ is the electron–phonon interaction matrix element. ω_ν is the frequency of an emitted phonon, and Γ is the spectral width. The Raman intensity is given by $I = |F|^2$. The scattering amplitude consists of two electron–photon matrix elements and one electron–phonon matrix element. The electron–photon interaction is given by the $\mathbf{A} \cdot \nabla$ inner product, where \mathbf{A}

denotes the vector potential associated with light and the direction of \mathbf{A} is parallel to the polarization vectors \mathbf{e}_i and \mathbf{e}_s . Because the wavelength of the light is much longer than the atomic wave functions, we can take $\langle m|\mathbf{A}\cdot\nabla|l\rangle = \mathbf{A}\cdot\langle m|\nabla|l\rangle$, which is called the dipole approximation. Thus, when we consider the directions of \mathbf{A} as \mathbf{e}_i and \mathbf{e}_s , the expression of eq 16 becomes the Raman tensor (see eq S2 of the Supporting Information) by selecting $\frac{\partial}{\partial x}$, $\frac{\partial}{\partial y}$, or $\frac{\partial}{\partial z}$ from ∇ in eq 16. In addition, when we assumed $m' \sim m$ for the intermediate states for optical absorption and emission, we obtained $\langle f|\nabla|m'\rangle = \langle m|\nabla|l\rangle^*$, which means that the product of the two electron–photon matrix elements can be approximated to be a real value. On the contrary, the electron–phonon matrix element $\langle m'|H_{\text{el-ph}}|m\rangle$ can be a complex value when we sum the matrix elements over several intermediate states m as shown in Figure S1a. In addition, the origin of φ is the anisotropic oscillation in the directions of x and z . We obtain a non-zero value of α because BP has a complex Raman tensor whose matrix elements have different phases. When we consider multilayer BP, we expect more conduction bands, which is consistent with the experimental results that show that the shift of the angle becomes larger. In addition, when we increase E_L , we expect that there will be more intermediate states that enhance the contribution of helicity-changing Raman spectra for A_g modes, which is also consistent with the experimental results. We should mention that the calculation is performed for only monolayer BP while the experiment is done for multilayer BP. In multilayer BP, the conduction and valence band split into several energy subbands, and we should consider each contribution of the Raman scattering amplitude. However, the observed Raman spectra show only three Raman active modes for which we cannot discuss the contribution of each subband. Thus, although we do not obtain the perfect correspondence of the E_L dependence of helicity-changing or -conserving Raman spectra, the analysis works satisfactorily.

In summary, we report the helicity-resolved Raman spectra of few-layer BP using CPL. We find that the A_g Raman active modes show intensities for both $\sigma+\sigma+$ and $\sigma+\sigma-$ configurations, and the relative intensity depends on the thickness of BP, crystal orientation θ , and laser excitation energy E_L . When we observe the polarized Raman spectra as a function of the angle of the linear polarizer for the scattered light, the mixing of helicity-conserving and helicity-changing Raman spectra is expressed by a deflection angle, which can be explained by introducing the complex Raman tensor. First-principles calculations confirm the complex Raman tensor whose origin comes from the complex value of electron–phonon matrix elements in anisotropic materials. Using the polarization-resolved Raman scattering by circular polarization excitation, we can experimentally obtain the information for phase factor φ of BP, regardless of the sample thickness and excitation lasers, which is consistent with the calculated results.

■ ASSOCIATED CONTENT

SI Supporting Information

The Supporting Information is available free of charge at <https://pubs.acs.org/doi/10.1021/acs.jpcllett.1c03826>.

Raman resonance intensity of monolayer BP calculated by first-principles calculations (Figure S1), polar plots of the Raman intensities (Figures S2–S5), and fitted values of complex phase φ from the experimental data (Table S1) (PDF)

■ AUTHOR INFORMATION

Corresponding Authors

Riichiro Saito – Department of Physics, Tohoku University, Sendai 980-8578, Japan; orcid.org/0000-0002-3336-9985; Email: rsaito@flex.phys.tohoku.ac.jp

Lianming Tong – College of Chemistry and Molecular Engineering, Beijing Science and Engineering Center for Nanocarbons, Beijing National Laboratory for Molecular Sciences, Peking University, Beijing 100871, P. R. China; orcid.org/0000-0001-7771-4077; Email: tonglm@pku.edu.cn

Authors

Shiyi Han – College of Chemistry and Molecular Engineering, Beijing Science and Engineering Center for Nanocarbons, Beijing National Laboratory for Molecular Sciences, Peking University, Beijing 100871, P. R. China

Yan Zhao – College of Chemistry and Molecular Engineering, Beijing Science and Engineering Center for Nanocarbons, Beijing National Laboratory for Molecular Sciences, Peking University, Beijing 100871, P. R. China; Academy for Advanced Interdisciplinary Studies, Peking University, Beijing 100871, P. R. China

Nguyen Tuan Hung – Frontier Research Institute for Interdisciplinary Science, Tohoku University, Sendai 980-8578, Japan; orcid.org/0000-0003-4156-6230

Bo Xu – College of Chemistry and Molecular Engineering, Beijing Science and Engineering Center for Nanocarbons, Beijing National Laboratory for Molecular Sciences, Peking University, Beijing 100871, P. R. China; Academy for Advanced Interdisciplinary Studies, Peking University, Beijing 100871, P. R. China

Jin Zhang – College of Chemistry and Molecular Engineering, Beijing Science and Engineering Center for Nanocarbons, Beijing National Laboratory for Molecular Sciences, Peking University, Beijing 100871, P. R. China; orcid.org/0000-0003-3731-8859

Complete contact information is available at: <https://pubs.acs.org/doi/10.1021/acs.jpcllett.1c03826>

Author Contributions

S.H., Y.Z., and N.T.H. contributed equally to this work. S.H. and Y.Z. conceived the idea and designed the experiments. N.T.H. performed the theoretical calculations. S.H., N.T.H., R.S., and L.T. wrote the manuscript. S.H., Y.Z., and B.X. analyzed the experimental data. R.S., J.Z., and L.T. supervised the work. All of the authors discussed the results and commented on the manuscript.

Notes

The authors declare no competing financial interest.

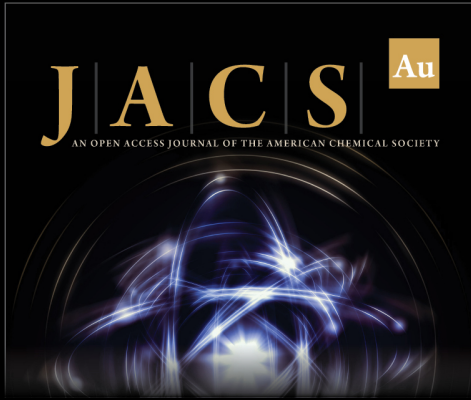
■ ACKNOWLEDGMENTS

The authors thank Prof. Qingliang Feng for helpful discussions. This work was financially supported by the Ministry of Science and Technology of China (2018YFA0703502 and 2016YFA0200104), the National Natural Science Foundation of China (Grants 51720105003, 21790052, 52021006, and 21974004), the Strategic Priority Research Program of CAS (XDB36030100), and the Beijing National Laboratory for Molecular Sciences (BNLMS-CXTD-202001). N.T.H. acknowledges JSPS KAKENHI Grant JP20K15178. R.S. acknowledges JSPS KAKENHI Grant JP18H01810 and the

Center for Science and Innovation in Spintronics (CSIS), Tohoku University.


REFERENCES


- (1) Liu, H.; Neal, A. T.; Zhu, Z.; Luo, Z.; Xu, X.; Tománek, D.; Ye, P. D. Phosphorene: An Unexplored 2D Semiconductor with a High Hole Mobility. *ACS Nano* **2014**, *8* (4), 4033–4041.
- (2) Castellanos-Gomez, A.; Vicarelli, L.; Prada, E.; Island, J. O.; Narasimha-Acharya, K. L.; Blanter, S. I.; Groenendijk, D. J.; Buscema, M.; Steele, G. A.; Alvarez, J. V.; et al. Isolation and Characterization of Few-Layer Black Phosphorus. *2D Mater.* **2014**, *1* (2), 025001.
- (3) Li, L.; Yu, Y.; Ye, G. J.; Ge, Q.; Ou, X.; Wu, H.; Feng, D.; Chen, X. H.; Zhang, Y. Black Phosphorus Field-Effect Transistors. *Nat. Nanotechnol.* **2014**, *9* (5), 372–377.
- (4) Xia, F.; Wang, H.; Hwang, J. C. M.; Neto, A. H. C.; Yang, L. Black Phosphorus and its Isoelectronic Materials. *Nat. Rev. Phys.* **2019**, *1* (5), 306–317.
- (5) Qiao, J.; Kong, X.; Hu, Z.-X.; Yang, F.; Ji, W. High-Mobility Transport Anisotropy and Linear Dichroism in Few-Layer Black Phosphorus. *Nat. Commun.* **2014**, *5* (1), 4475.
- (6) Buscema, M.; Groenendijk, D. J.; Blanter, S. I.; Steele, G. A.; van der Zant, H. S. J.; Castellanos-Gomez, A. Fast and Broadband Photoresponse of Few-Layer Black Phosphorus Field-Effect Transistors. *Nano Lett.* **2014**, *14* (6), 3347–3352.
- (7) Tran, V.; Soklaski, R.; Liang, Y.; Yang, L. Layer-Controlled Band Gap and Anisotropic Excitons in Few-Layer Black Phosphorus. *Phys. Rev. B* **2014**, *89* (23), 235319.
- (8) Li, L.; Kim, J.; Jin, C.; Ye, G. J.; Qiu, D. Y.; da Jornada, F. H.; Shi, Z.; Chen, L.; Zhang, Z.; Yang, F.; et al. Direct Observation of the Layer-Dependent Electronic Structure in Phosphorene. *Nat. Nanotechnol.* **2017**, *12* (1), 21–25.
- (9) Wu, J.; Koon, G. K. W.; Xiang, D.; Han, C.; Toh, C. T.; Kulkarni, E. S.; Verzhbitskiy, I.; Carvalho, A.; Rodin, A. S.; Koenig, S. P.; et al. Colossal Ultraviolet Photoresponsivity of Few-Layer Black Phosphorus. *ACS Nano* **2015**, *9* (8), 8070–8077.
- (10) Wang, X.; Lan, S. Optical Properties of Black Phosphorus. *Adv. Opt. Photon.* **2016**, *8* (4), 618–655.
- (11) Tatsumi, Y.; Kaneko, T.; Saito, R. Conservation Law of Angular Momentum in Helicity-Dependent Raman and Rayleigh Scattering. *Phys. Rev. B* **2018**, *97* (19), 195444.
- (12) Saito, R.; Tatsumi, Y.; Huang, S.; Ling, X.; Dresselhaus, M. S. Raman Spectroscopy of Transition Metal Dichalcogenides. *J. Phys.: Condens. Matter* **2016**, *28* (35), 353002.
- (13) Tatsumi, Y.; Saito, R. Interplay of Valley Selection and Helicity Exchange of Light in Raman Scattering for Graphene and MoS₂. *Phys. Rev. B* **2018**, *97* (11), 115407.
- (14) Drapcho, S. G.; Kim, J.; Hong, X.; Jin, C.; Shi, S.; Tongay, S.; Wu, J.; Wang, F. Apparent Breakdown of Raman Selection Rule at Valley Exciton Resonances in Monolayer MoS₂. *Phys. Rev. B* **2017**, *95* (16), 165417.
- (15) Chen, S.-Y.; Zheng, C.; Fuhrer, M. S.; Yan, J. Helicity-Resolved Raman Scattering of MoS₂, MoSe₂, WS₂, and WSe₂ Atomic Layers. *Nano Lett.* **2015**, *15* (4), 2526–2532.
- (16) Saito, R.; Ukhtary, M. S.; Wang, S. K.; Hung, N. T. Selection Rule for Raman Spectra of Two-Dimensional Materials Using Circularly-Polarized Vortex Light. *Phys. Chem. Chem. Phys.* **2021**, *23* (32), 17271–17278.
- (17) Zhao, Y.; Xu, B.; Tong, L.; Zhang, J. The Helicity of Raman Scattered Light: Principles and Applications in Two-Dimensional Materials. *Sci. China Chem.* **2022**, *65*, 269.
- (18) Sugai, S.; Ueda, T.; Murase, K. Pressure Dependence of the Lattice Vibration in the Orthorhombic and Rhombohedral Structures of Black Phosphorus. *J. Phys. Soc. Jpn.* **1981**, *50* (10), 3356–3361.
- (19) Sugai, S.; Shirovani, I. Raman and Infrared Reflection Spectroscopy in Black Phosphorus. *Solid State Commun.* **1985**, *53* (9), 753–755.
- (20) Kaneta, C.; Katayama-Yoshida, H.; Morita, A. Lattice Dynamics of Black Phosphorus. I. Valence Force Field Model. *J. Phys. Soc. Jpn.* **1986**, *55* (4), 1213–1223.
- (21) Liu, S. J.; Huo, N. J.; Gan, S.; Li, Y.; Wei, Z. M.; Huang, B. J.; Liu, J.; Li, J. B.; Chen, H. D. Thickness-Dependent Raman Spectra, Transport Properties and Infrared Photoresponse of Few-Layer Black Phosphorus. *J. Mater. Chem. C* **2015**, *3* (42), 10974–10980.
- (22) Ribeiro, H. B.; Pimenta, M. A.; de Matos, C. J. S.; Moreira, R. L.; Rodin, A. S.; Zapata, J. D.; de Souza, E. A. T.; Castro Neto, A. H. Unusual Angular Dependence of the Raman Response in Black Phosphorus. *ACS Nano* **2015**, *9* (4), 4270–4276.
- (23) Resende, G. C.; Ribeiro, G. A. S.; Silveira, O. J.; Lemos, J. S.; Brant, J. C.; Rhodes, D.; Balicas, L.; Terrones, M.; Mazzoni, M. S. C.; Fantini, C.; et al. Origin of the Complex Raman Tensor Elements in Single-Layer Triclinic ReSe₂. *2D Mater.* **2021**, *8* (2), 025002.
- (24) Yokota, M. Polarization Analysis by Off-Axis Digital Holography with an Improved Optical System and an Evaluation of its Performance by Simulation. *Appl. Opt.* **2008**, *47* (34), 6325–6333.



JACS Au
AN OPEN ACCESS JOURNAL OF THE AMERICAN CHEMICAL SOCIETY

Editor-in-Chief
Prof. Christopher W. Jones
Georgia Institute of Technology, USA

Open for Submissions 

pubs.acs.org/jacsau  ACS Publications
Most Trusted. Most Cited. Most Read.